Phase diagram of the partly filled honeycomb lattice in AgCrS₂-like solid ionic conductors

T. Hibma and S. Strässler

Brown Boveri Research Center, CH-5405 Baden, Switzerland

(Received 4 February 1983)

The phase diagram of the two-dimensional system of conduction ions in layered solid electrolyte materials based on $AgCrS_2$ was determined experimentally and found to be strongly asymmetric with respect to the half-filled lattice. Lattice-gas theory with pairwise interactions predicts a symmetric phase diagram. As an example, the phase diagram for the honeycomb lattice is calculated using the cluster-variation method with a hexagon as a basic cluster and first- and second-neighbor interactions. The pronounced deviation from simple lattice-gas theory is attributed to the liquidlike character of the conduction-ion subsystem. In a lattice-gas type of calculation, the relaxation effects typical for solid electrolytes may be taken care of by introducing many-body interactions. This is illustrated by a cluster-variation calculation with a star as a basic cluster. The shape of the experimental phase diagram can be formally reproduced if large clusters of vacant sites are excluded, suggesting that the relaxation effects of the framework of nonconducting ions are dominating the many-body interactions.

I. INTRODUCTION

In solid electrolytes the conduction-ion subsystem is in a highly disordered state, having lattice-gas as well as liquidlike aspects.[1] On account of the framework of immobile ions, a periodic background potential and therefore a well-defined sublattice exists. In lattice-gas theory, the ions are distributed over the lattice points, defined as the minima of the background potential, the local order of the ions being determined by their interactions. However, the assumption of a discrete lattice implies that the potential wells are deep, whereas, in fact, in solid electrolytes the potential barriers between neighboring sites are low to assure a high mobility of the conduction ions. A consequence of the flatness of the potential is that ionic relaxations play a very important role and give the conduction-ion subsystem a liquidlike character.

In Ref. 1 a generalized lattice-gas description of a solid electrolyte is proposed in which these relaxation effects are included. This theory has been used to calculate the static and dynamical properties of a partly occupied equidistant one-dimensional lattice, as it is found in one-dimensional conductors of the Hollandite type.[2] For a given form of the periodic background and interaction potential, the displaced positions of the ions in all possible configurations on a linear equidistant lattice of finite length were calculated as well as all individual configurational energies. As compared to a discrete lattice-gas model, the most important consequences of the inclusion of displacement disorder were the following: an appreciable reduction of the energy of the most probable configurations, a reduction of the effective potential barrier for configurations important for the conduction process, and a reduction of the number of stable configurations (configuration quenching). The latter phenomenon is observed if the displacements in the particular configurations exceed the distance between a lattice site and the potential barrier.

A similar rigorous calculation for a two- or three-dimensional lattice would be far too complex, and more approximate procedures have to be found to take care of relaxation effects. In this paper we want to show that a straightforward way to do this is offered by the cluster-variation (CV) method of Kikuchi.[3] This method is basically a lattice-gas approach in which relaxation effects can be taken into account by introducing many-body interactions and configuration quenching by neglecting extreme cluster configurations. We will apply these ideas to two-dimensional solid electrolyte compounds based on $AgCrS_2$. In particular, we will try to simulate the main features of the phase diagram of the conduction-ion subsystem.

$AgCrS_2$ has a layer structure in which the silver ions occupy half of the sites on a puckered honeycomb lattice situated between CrS_2^- "sandwiches" (Fig. 1). The material shows an order-disorder transition at 673 K (Refs. 4 and 5) from an ordered phase in which only one of the two triangular sublattices of the honeycomb lattice is occupied, to a disordered phase in which all sites are occupied with equal probability. By means of chemical substitutions into the CrS_2^- framework, the occupancy of the silver sublat-
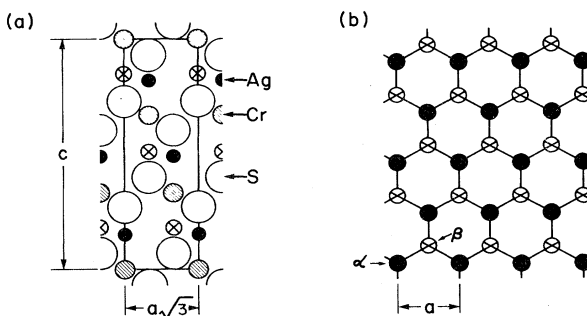

FIG. 1. (a) Structure of $AgCrS_2$ is rhombohedral and consists of alternating silver, sulfur, chromium, and sulfur layers. (b) Tetrahedrally coordinated sites for the silver ions build a puckered honeycomb lattice. At low temperatures only the α sublattice is occupied; above the order-disorder transition temperature at 673 K both triangular sublattices are occupied.

tice may be varied and consequently the phase diagram of the silver subsystem, i.e., the critical temperature as a function of the occupancy of the lattice, can be determined.

In Sec. II we will describe the preparation and characterization of the chemically modified $AgCrS_2$-based materials. The results of the measurements of the order-disorder transition temperature for these materials are given in Sec. III. A characteristic feature of the experimental phase diagram is its pronounced asymmetry around the half-filled lattice. As will be argued in Sec. IV, this feature is associated with the specific nature of the disorder in a solid electrolyte. In Sec. V the phase-diagram calculation using the CV method is presented. First, a conventional discrete lattice-gas type of calculation is carried out, assuming pairwise interactions and taking a hexagon as a basic cluster. For the calculation of the asymmetric phase diagram, a different cluster, the star, is chosen to allow the introduction of the most relevant many-body interactions. The results of this calculation are compared with the experimental phase diagram in Sec. VI.

II. MATERIALS

$AgCrS_2$ is essentially a stoichiometric compound.[4] From coulometric titration measurements, using AgI as a solid silver-ion conductor, the stoichiometry range for silver at the phase-transition temperature is only a few per mil. To determine the phase diagram of the silver subsystem, a much larger variation is necessary. This was accomplished by substituting the ions of the CrS_2^- framework with ions having approximately the same size, but a different valency. Suitable substitutions were found to be V, Ti, or Sn for Cr, and Cl for S.

The materials were prepared by heating a mixture of the elements in evacuated silica tubes at 1000 °C for several days and cooling down slowly. In the case of the Cl-substituted materials, small amounts of AgCl or $CrCl_3$ were added. Guinier x-ray photographs were used to check whether the materials had the same crystal structure as $AgCrS_2$, and to measure the lattice constants. The development of the lattice parameter for the hexagonal plane (a) is shown in Fig. 2. The x-ray pictures also showed whether second phases like silver metal, silver sulfide, or transition-metal sulfides were present. In addition, specific-heat measurements were used to detect small quantities of elemental sulfur and Ag_2S. The specific-heat measurements were performed using a Perkin-Elmer differential scanning calorimeter II.

As might be expected, the substitutions lead to silver-deficient materials. With the exception of the V-substituted material, the silver content is close to $1-x$, x being the fraction of substituted ions. The stoichiometry range for silver increases with increasing degree of substitution but stays narrow. The maximum rates of substitution were approximately 0.25 for Ti and Sn, and 0.1 for Cl.

The V-substituted materials behaved quite differently. The stoichiometry range for Ag increased strongly with increasing degree of substitution. For a fixed V content, the Ag content can be varied between a value larger than
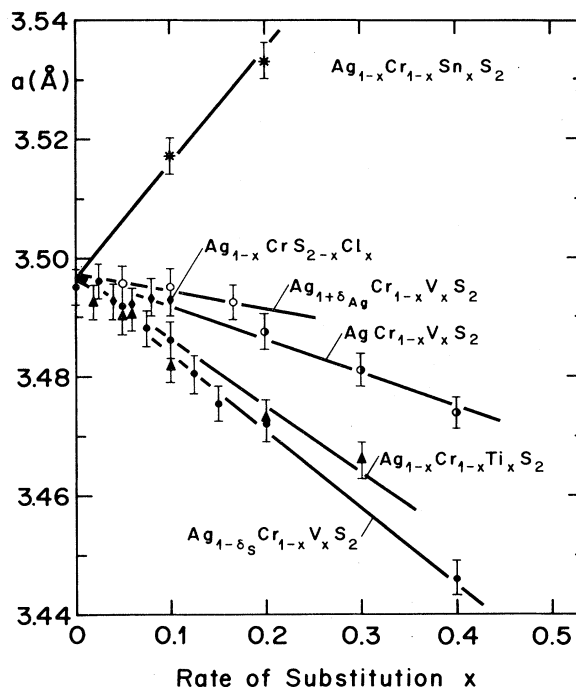

FIG. 2. Lattice parameter a of the hexagonal plane for the chemically modified $AgCrS_2$-based materials as a function of the rate of substitution x.

but close to $1-x$ and a value slightly exceeding 1. At least half of the Cr ions can be substituted with V ions without a change in structure or the appearance of a second phase. Attempts to introduce foreign cations with a valency smaller than 3 were unsuccessful.

III. EXPERIMENTAL PHASE DIAGRAMS

Order-disorder transition temperatures were determined from specific-heat measurements. As an example, the specific-heat curve of $AgCrS_2$ is shown in Fig. 3. The critical temperature (T_c) was taken to be the position of the maximum of the specific-heat anomaly. In Fig. 4 the
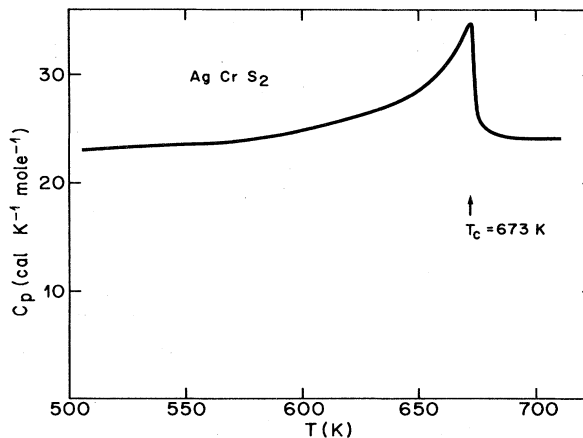

FIG. 3. Specific heat of $AgCrS_2$. The anomalous structure at 673 K is due to the order-disorder transition of the silver ions.
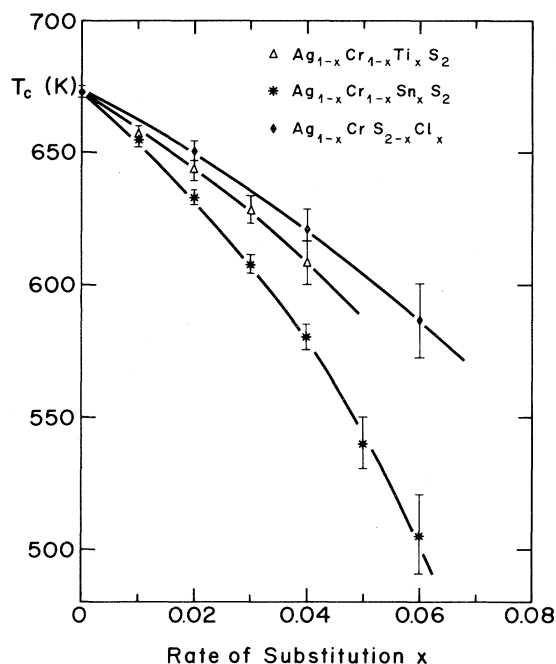
FIG. 4. Order-disorder transition temperature as a function of the rate of substitution in the CrS_2^- framework for Ti, Sn, and Cl substitutions.

FIG. 5. Order-disorder transition temperature as a function of the rate of substitution of Cr by V in $AgCrS_2$, for samples in equilibrium with silver metal, samples with a fixed silver content of 1, and samples in equilibrium with silver sulfide and sulfur.

ing the critical temperatures to the one for the half-filled lattice. All the curves have in common that the critical temperature increases very strongly with increasing silver density. In fact, the data fall approximately on a single master curve with the exception of the Sn-substituted material. This similarity shows that the functional shape of

critical temperature as a function of the silver density is shown for the compounds $Ag_{1-x}(Cr_{1-x}Ti_x)S_2$, $Ag_{1-x}(Cr_{1-x}Sn_x)S_2$, and $Ag_{1-x}Cr(S_{2-x}Cl_x)$. The range of measurement on the low-density side is limited by the broadening of the specific-heat anomaly with increasing silver deficiency. For the V-substituted material, the variation of the critical temperature with the degree of substitution is shown for three cases (Fig. 5): (a) samples in equilibrium with silver sulfide and sulfur, having the lowest possible silver content, which are larger than but close to $1-x$ $[Ag_{1-\delta S}(Cr_{1-x}V_x)S_2]$, (b) samples with a fixed silver content of 1 $[Ag(Cr_{1-x}V_x)S_2]$, and (c) samples in equilibrium with metallic silver having the highest possible silver content, which is somewhat larger than 1 $[Ag_{1+\delta Ag}(Cr_{1-x}V_x)S_2]$. The broad stoichiometry range for silver in this case offers the possibility to determine the variation of the critical temperature as a function of the silver density for a fixed rate of V substitution (δ_0). Starting from silver-deficient samples, small amounts of silver metal were added and dissolved by heating to temperatures slightly above the transition temperature. This was done for three values of δ_0: 0.05, 0.1, and 0.2. The critical temperature versus silver-density curves are shown in Fig. 6.

We therefore dispose of six curves representing the phase diagram of the silver subsystem in a $AgCrS_2$-type layer structure, three in which the silver density was changed parallel to the chemical substitution into the framework (the Ti-, Sn- and Cl-substituted materials), and three in which the degree of substitution was kept fixed and only the silver content was changed (the V-substituted materials). In Fig. 7 these data are compared by normaliz-
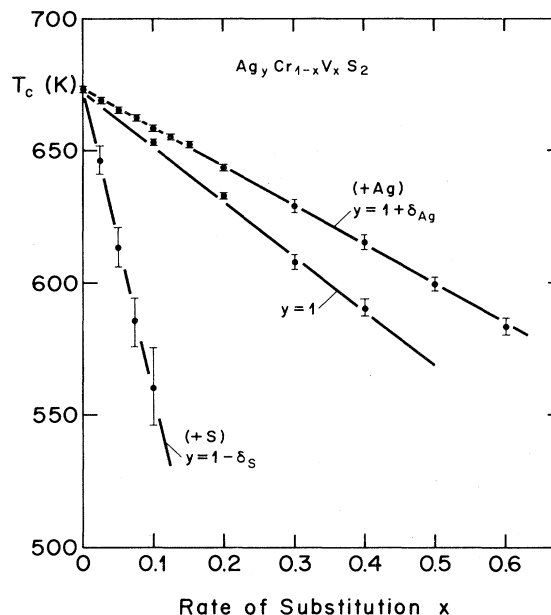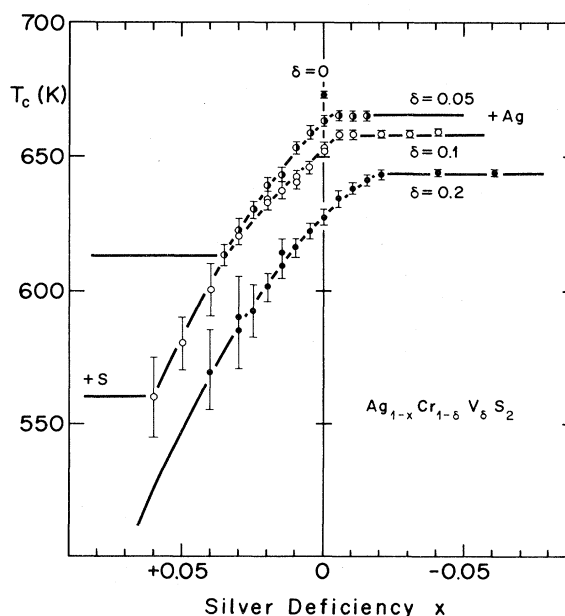

FIG. 6. Order-disorder transition temperature for V-substituted $AgCrS_2$ as a function of the silver deficiency for three fixed V contents: $\delta = 0.05$, 0.1, and 0.2.
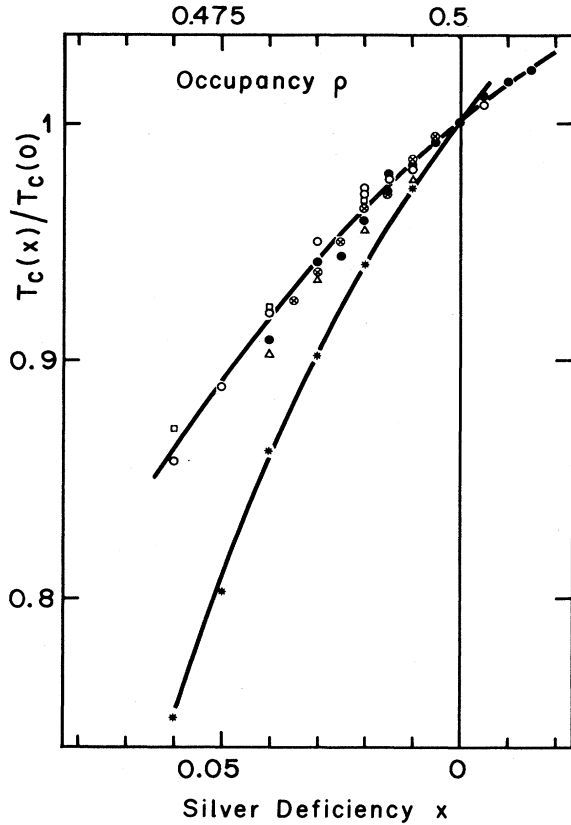
FIG. 7. Phase diagram of the silver subsystem in $AgCrS_2$-based materials as a function of the occupancy ρ of the honeycomb lattice [$Ag_{1-x}Cr_{1-\delta}V_\delta S_2$, $\delta=0.05$ ($\otimes$), 0.1 ($\bigcirc$), and 0.2 ($\bullet$); $Ag_{1-x}Cr_{1-x}Ti_xS_1$ ($\triangle$); $Ag_{1-x}Cr_{1-x}Sn_xS_2$ ($*$) and $Ag_{1-x}CrS_{2-x}Cl_x$ ($\square$)]. The transition temperatures have been normalized to the one for the half-filled lattice.

the phase diagram is more or less independent of the nature of the chemical changes in the transition-metal dichalcogenide framework.

IV. ASYMMETRY OF THE PHASE DIAGRAM

For constant pairwise interactions, no matter how long range they are, lattice-gas theory predicts a symmetric phase diagram around the half-filled lattice.[6] This symmetry is a result of the particle-hole equivalence in the free-energy expression. The experimental phase diagrams of Fig. 7, however, are very asymmetric, i.e., the slope of the normalized critical temperature at $\rho=\frac{1}{2}$ is very different from zero, i.e.,

$$\left| \frac{1}{T_c} \frac{dT_c}{d\rho} \right|_{\rho=1/2} \cong 3.0 \qquad (1)$$

for all but the Sn-substituted case, for which a value of about 5.5 is obtained. As was pointed out in the Introduction, strong deviations from a discrete lattice-gas theory are indeed expected because of the liquidlike aspects of solid electrolytes. It is therefore natural to associate the asymmetry of the phase diagram with relaxation effects

typical for these materials. A number of alternative mechanisms, however, might be of importance as well and will be discussed first.

A more or less trivial cause for the asymmetry of the phase diagram would be a dependence of the pairwise potentials on the silver density. The variation of the silver content in our systems is necessarily accompanied by changes in the chemical composition and the electronic structure of the framework of nonconducting ions. These changes will influence the pairwise interactions through the interionic distance, the ionic charge, and the dielectric constant. The effect of the change in the lattice parameter can by ruled out by a rough estimate, using the data of Fig. 2. Besides the fact that with exception of the Sn case, the wrong sign is predicted for the slope of the phase diagram at $\rho=\frac{1}{2}$, the magnitude of the lattice expansion or contraction is much too small to be of importance. Similarly, small changes in the rate of charge transfer from the silver atoms to the transition-metal dichalcogenide layers can neither explain the sign nor the magnitude of this slope. A more serious factor is the change in the electronic screening of the interactions of the mobile ions by the changes in the electronic structure of the framework. To check this possibility, we have determined the optical dielectric constant from the optical reflectivity of polished pellets of the chemically modified materials as compared to pure $AgCrS_2$ in the infrared region between 1000 and 4000 cm^{-1}. To minimize the reduction of the signal by surface roughness, the value at 1000 cm^{-1} was taken. For the silver-deficient samples a small but distinct increase in the reflectivity was observed. For $x=0.1$, values around 0.190 were obtained as compared to 0.185 for pure $AgCrS_2$. The corresponding increase in the dielectric constant is from 6.3 to 6.5. This increase is at least a factor of 5 too small to explain the observed slope of the phase diagram. It does explain the decrease in the critical temperature with the increasing rate of V substitution for a constant silver content of 1 [the $Ag(Cr_{1-x}V_x)S_2$ series in Fig. 5].

The above arguments ascertain that local relaxation effects are responsible for the asymmetry of the phase diagram. In fact, there is ample independent experimental evidence for the importance of these phenomena in $AgCrS_2$, from diffuse x-ray,[7] far-infrared, and inelastic neutron scattering data.[8]

The diffuse x-ray pattern of $AgCrS_2$ in the disordered state is characteristic for a two-dimensional liquid. The radial distribution function shows a first peak at 3.0 Å, as compared to the first-neighbor distance on the honeycomb lattice of 2.0 Å, suggesting a considerable average displacement of the silver ions.

Far-infrared and inelastic neutron scattering measurements show that very low-frequency modes of vibration exist, involving the motion of the silver ions in directions parallel to the layers, suggesting that the potential wells for these ions are relatively shallow. The frequency of the optically active mode decreases strongly with temperature, showing that anharmonic contributions to the potential play a significant part even at very low temperatures. A shallow potential surface favors the displacement relaxation of the conduction ions.

The relaxation effects are not restricted to the silver subsystem. If the framework of nonconducting ions is not

rigid but highly polarizable as is the case for the chalcogenide compounds we studied, relaxation effects in the framework will be induced by a local excess or deficiency of conduction ions in the disordered state. These relaxations must be taken care of as well in the description of the state of order of the system.

Independent of their nature, the local relaxation effects may be formally included in a lattice-gas model by introducing many-body interactions. A very convenient formalism to treat these interactions is the CV method developed by Kikuchi.[3] The many-body contributions are simply introduced by assigning individual interaction energies to all different configurations of the basic cluster. The method can be applied to complicated lattices, and elegant iteration procedures have been developed recently[9,10] to simplify the calculational problems for large clusters. It has recently been used with considerable success to calculate rather complicated phase diagrams of binary and ternary systems with first- and second-neighbor interactions.[10-13] In the next section we will apply the method to the honeycomb lattice. As a reference, we will first calculate the phase diagram for pairwise interactions and subsequently introduce many-body interactions in the calculation in order to simulate the asymmetry of the phase diagram.

V. PHASE-DIAGRAM CALCULATION

In the CV method the configurational entropy is approximated by

$$S = k_B \ln \Omega ,$$ (2a)

$$\Omega = \prod_r \prod_l [x(r,l)N!]^{\gamma(r)} ,$$ (2b)

where k_B is the Boltzmann constant, N is the number of lattice points, Ω is the number of configurations, and $x(r,l)$ is the probability of occurrence of a particular configuration l on the cluster of sites of type r. The coefficient $\gamma(r)$ may be calculated from[10]

$$\gamma(r) = N(r)/N - \sum_q n(r,q)\gamma(q) ,$$ (3)

where $N(r)$ is the total number of different r clusters of the lattice and $n(r,q)$ is the number of q clusters in which the r clusters can be decomposed. Starting with the basic cluster n for which $\gamma(n) = N(n)/N$, the $\gamma(r)$ of successively smaller subclusters are easily calculated from Eq. (3). Only those subclusters have nonzero $\gamma(r)$, which are identical to the overlap regions of the larger clusters.[10]

The choice of the basic cluster depends on the range of the interaction potentials and the degree of approximation wanted. The simplest approximation in which the first-neighbor pair is chosen as the basic cluster is identical to the well known quasichemical approximation.[14] For first-neighbor interactions, improved results can only be expected if the basic cluster is a so-called closed cluster, i.e., a cluster which contains no points belonging to only one of the principal overlap clusters, because open clusters give results which are identical to those for its largest closed subcluster.[15] For the honeycomb lattice, the smallest closed cluster larger than a pair is the hexagon. All smaller three-, four-, or five-point clusters contain singly

connected points and are therefore open clusters. The hexagon seems to be a reasonable choice, because also second- and third-neighbor interactions may be included. In principle, many ordered structures on the honeycomb lattice might be dealt with, using one or more different types of hexagons. Because we are interested in the order-disorder transition for the close to half-filled honeycomb lattice, we will restrict our calculations to these two phases, and only one hexagon with alternating α and β sites has to be considered.

As was pointed out in the preceding section, pairwise interactions lead to a symmetric phase diagram, and many-body interactions have to be introduced to simulate the extreme asymmetry of the experimental phase diagram. The hexagon is not the most appropriate cluster to do this. Preferably, the basic cluster should contain a lattice point and all its first neighbors. The smallest cluster of this kind is the four-point cluster consisting of a central ion and its three neighbors, which we will call a star (see Fig. 8). Note that this cluster is an open cluster with respect to first-neighbor bonds, and the results for first-neighbor interactions will reduce to those for the pair approximation.

For both the hexagon and the star, the next largest overlap cluster is the first-neighbor pair. The subclusters to be considered are therefore only pairs and points. In Table I we have listed the values for the numbers $N(r)/N$ and $n(r,q)$ for the hexagon, star, first-neighbor pair, and point clusters. Note that the number of lattice points was taken to be $2N$ to avoid nonintegral quantities. Also listed are the values for the coefficients $\gamma(r)$ for the pair (Y), star (S), and hexagon (H) approximation, calculated using Eq. (3). The number of configurations for the various approximations are as follows:

$$\Omega_Y = X^4/Y^3 ,$$ (4a)

$$\Omega_S = Y^3/S^2 ,$$ (4b)

$$\Omega_H = Y^3/HX^2 ,$$ (4c)

where

$$X = \prod_i (x_i N!) ,$$ (5a)

$$Y = \prod_{i,j} (y_{ij} N!) ,$$ (5b)

$$S = \prod_{i,j,k,l} (s_{ijkl} N!) ,$$ (5c)

$$H = \prod_{i,j,k,l,m,n} (h_{ijklmn} N!) .$$ (5d)

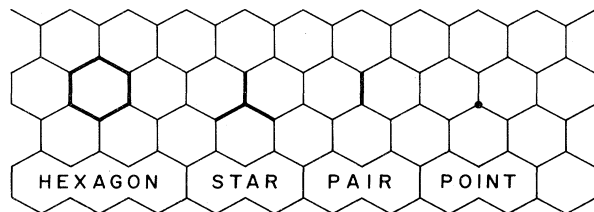The indices take on a value of 1 if the corresponding site

FIG. 8. Clusters used in the CV calculations.

TABLE I. Quantities needed for the calculation of the entropy in the CV approximation on a honey-comb lattice with a hexagon (H), star (S), or pair (Y) as a basic cluster [Eqs. (2) and (3)].

| r | $N(r)/N$ | $n(r,q)$ | | | | $\gamma_H(r)$ | $\gamma_S(r)$ | $\gamma_Y(r)$ |
		$q=H$	$q=S$	$q=Y$	$q=X$			
hexagon (H)	1	1	0	0	0	1		
star (S)	2	0	1	0	0	0	2	
pair (Y)	3	6	3	1	0	-3	-3	3
point (X)	2	6	4	2	1	2	0	-4

is occupied and 0 if it is empty.

A straightforward procedure would be to minimize the free energy

$$F=E-Nk_BT\sum_{r=1}^{n}\gamma(r)\sum_l x(r,l)\ln[x(r,l)] ,\qquad(6)$$

with respect to all independent configuration variables, which may be found by considering all conditions connecting the configuration probabilities occurring in Eq. (6). A more convenient method for larger clusters, however, is the natural-iteration method of Kikuchi,[9] in which the grand potential

$$G=F-\mu\rho N\qquad(7)$$

is minimized with respect to all basic cluster variables. The subsidiary conditions among the parameters are taken care of as completely as possible by writing the free energy in its most symmetric form, and if necessary, by adding the corresponding Lagrange terms to the expression for the grand potential.[16] In many cases it is sufficient to add the normalization condition, i.e.,

$$G=F-\mu\rho N+\lambda N\left[1-\sum_l x(n,l)\right] .\qquad(8)$$

Differentiation with respect to the $x(n,l)$ leads to the so-called superposition equations, expressing the basic cluster variables as powers of the subcluster variables and an exponential containing the energy and Lagrangian parameters as well as the chemical potential. For a fixed chemical potential and temperature, these equations are solved by iteration, and the phase with the lowest grand potential is the more stable phase. The critical temperature for a second-order phase transition is determined by the condition that the determinant of the matrix of second derivatives of the free energy with respect to the order parameters vanishes.

A. Pair approximation

For the ordered phase around $\rho=\frac{1}{2}$ on a honeycomb lattice there are two sublattices α and β as shown in

Fig. 1, each consisting of N sites. The first-neighbor interaction energy can be written as

$$\epsilon_{ij}=\epsilon ij .\qquad(9)$$

The conditions

$$x_i^{\alpha}=\sum_j y_{ij} ,\quad x_i^{\beta}=\sum_j y_{ji}\qquad(10)$$

may be accounted for by writing the superposition expression in the form,[9]

$$y_{ij}=(x_i^{\alpha}x_j^{\beta})^{2/3}\exp\{[2\lambda+\mu(i+j)-3\epsilon_{ij}]/3k_BT\} .\qquad(11)$$

These equations may be solved by applying the natural-iteration method, i.e., trial values for x_i^{α} and x_i^{β} are used to calculate y_{ij} from Eq. (11), and new values for x_i^{α} and x_i^{β} are than determined from Eqs. (10). This procedure is repeated until the changes after each new iteration cycle are sufficiently small.

In this case, however, an analytical expression for the phase diagram may be derived by conventional procedures,[14] reading

$$\frac{\epsilon}{k_BT_c}=\ln\frac{9\rho(1-\rho)}{(3\rho-1)(2-3\rho)} ,\qquad(12)$$

where ρ is the occupancy of the lattice and T_c is the critical temperature.

B. Hexagon approximation

We define hexagon probabilities h_{ijklmn}, for which the first, third, and fifth index are associated with an α site and the remaining ones with a β site. The subsidiary conditions

$$y_{ij}=\sum_{k,l,m,n}h_{ijklmn}=\sum_{k,l,m,n}h_{klijmn}=\sum_{k,l,m,n}h_{klmnij}\qquad(13)$$

as well as Eqs. (10) are again taken care of by the symmetry of the superposition equation:

$$h_{ijklmn}=\frac{(y_{ij}y_{kl}y_{mn}y_{in}y_{kj}y_{ml})^{1/2}}{(x_i^{\alpha}x_j^{\beta}x_k^{\alpha}x_l^{\beta}x_m^{\alpha}x_n^{\beta})^{1/3}}\exp\left[\frac{2\lambda+\mu(i+j+k+l+m+n)/3-\epsilon_{ijklmn}}{k_BT}\right] ,\qquad(14)$$

where

$$\epsilon_{ijklmn}=\epsilon_1(ij+jk+kl+lm+mn+ni)/2+\epsilon_2(ik+jl+km+ln+mi+nj)+\epsilon_3(il+jm+kn)\qquad(15)$$

and ϵ_1, ϵ_2, and ϵ_3 are the first-, second- and third-neighbor interactions. These equations can be solved by an iteration procedure similar to the one described for the pair approximation.

For first-neighbor interactions only ($\epsilon_1 \neq \epsilon_2 = \epsilon_3 = 0$), the phase limits at low temperatures are at $\rho = 0.5 \pm 0.123$ (see Fig. 9). For the pair approximation these limits are at $\rho = \frac{1}{3}$, and $\frac{2}{3}$, respectively. The improvement of the hexagon over the pair approximation is considerable if the values for $k_B T_c / \epsilon_1$ for the half-filled lattice are compared with the exact result: 0.455 12 for the pair, 0.402 30 for the hexagon approximation, and 0.379 66 for the exact solution.[17]

If second-neighbor interactions are also different from zero, the most remarkable change is the low-temperature behavior. In the limit of 0 K, the ordered phase is only stable at $\rho = \frac{1}{2}$. The ratio $k_B T_c / \epsilon_1$ at the half-filled lattice decreases with increasing ϵ_2 until the ordered phase disappears completely for $\epsilon_2 / \epsilon_1 \gtrsim 0.25$. The fact that the ordered structure considered here is observed experimentally shows that in AgCrS$_2$ the second-neighbor interaction must be considerably smaller than the first-neighbor interaction. This is a reasonable result because a pair of first-neighbor silver ions "touch" so that the core repul-

sion contributes considerably to the first-neighbor interaction.

C. Star approximation

Two different kinds of star-configuration probabilities are to be defined, s_{ijkl}^α and s_{ijkl}^β. The first index is associated with the central α or β site, respectively. The subsidiary conditions are

$$y_{ij} = \sum_{k,l} s_{ijkl}^\alpha = \sum_{k,l} s_{ikjl}^\alpha = \sum_{k,l} s_{iklj}^\alpha , \tag{16a}$$

$$y_{ji} = \sum_{k,l} s_{ijkl}^\beta = \sum_{k,l} s_{ikjl}^\beta = \sum_{k,l} s_{iklj}^\beta , \tag{16b}$$

and Eqs. (10). The permutation symmetry among j, k, and l again can be accounted for by writing the superposition equations in the appropriate form. However, the relation between star probabilities around α and β sites have to be dealt with separately by adding the following terms to the grand potential:

$$\sum_{i,j,k,l} [(a_{ij} + a_{ik} + a_{il})s_{ijkl}^\alpha - (a_{ji} + a_{ki} + a_{li})s_{ijkl}^\beta] ,$$

where the a_{ij} are the Lagrangian coefficients. Differentiation with respect to the star-configuration probabilities gives the following superposition expressions:

$$s_{ijkl}^\alpha = (y_{ij} y_{ik} y_{il})^{1/2} \exp\left[\frac{\lambda + \mu(i+j+k+l)/4 - \epsilon_{ijkl} + a_{ij} + a_{ik} + a_{il}}{2k_B T} \right] , \tag{17a}$$

$$s_{ijkl}^\beta = (y_{ji} y_{ki} y_{li})^{1/2} \exp\left[\frac{\lambda + \mu(i+j+k+l)/4 - \epsilon_{ijkl} - a_{ji} - a_{ki} - a_{li}}{2k_B T} \right] . \tag{17b}$$

For the Lagrangian multipliers the following equations may be derived using Eqs. (16) and (17):

$$a_{ij} = \frac{1}{2} k_B T \ln\left[\frac{\sum_{k,l} (y_{kj} y_{lj})^{1/2} \exp\{[\frac{1}{4}\mu(k+l) - \epsilon_{jikl} - a_{kj} - a_{lj}]/2k_B T\}}{\sum_{k,l} (y_{ik} y_{il})^{1/2} \exp\{[\frac{1}{4}\mu(k+l) - \epsilon_{ijkl} + a_{ik} + a_{il}]/2k_B T\}} \right] . \tag{18}$$

Each major iteration cycle using Eqs. (16) and (17) is followed by a minor iteration cycle[16] to determine the Lagrangian multipliers from (18), either by calculating the a_{ij} on the left-hand side using the old values on the right-hand side, or by applying the Newton-Raphson method.[18]

Before discussing some of the solutions of the general case, we will prove that, if only first-neighbor interactions are taken into account, i.e., if

$$\epsilon_{ijkl} = \epsilon_1(ij + ik + il) , \tag{19}$$

the star approximation is identical with the pair approximation. Expression (19) allows us to write the superposition equations in the following form:

$$s_{ijkl}^\alpha = z_{ij}^\alpha z_{ik}^\alpha z_{il}^\alpha, \quad s_{ijkl}^\beta = z_{ji}^\beta z_{ki}^\beta z_{li}^\beta , \tag{20}$$

where

$$z_{ij}^\alpha = (y_{ij})^{1/2} \exp\left[\frac{\lambda + \mu(i+3j)/4 + 3\alpha_{ij} - 3\epsilon ij}{6k_B T} \right] , \tag{21a}$$

$$z_{ij}^\beta = (y_{ij})^{1/2} \exp\left[\frac{\lambda + \mu(j+3i)/4 + 3\alpha_{ij} - 3\epsilon ij}{6k_B T} \right] . \tag{21b}$$

The subsidiary conditions (10) can now be written as

$$x_i^\alpha = \left[\sum_j z_{ij}^\alpha \right]^3, \quad x_i^\beta = \left[\sum_j z_{ji}^\beta \right]^3 , \tag{22}$$

and Eqs. (16), together with Eqs. (20) and (22), as

$$y_{ij} = z_{ij}^\alpha (x_i^\alpha)^{2/3}, \quad y_{ji} = z_{ji}^\beta (x_i^\beta)^{2/3} . \tag{23}$$

Elimination of the α_{ij} from the latter equations leads to the superposition expression for the pair approximation [Eq. (11)].

Up to this point we have only discussed the phase diagram for the case of pairwise interactions. We will now introduce three- and four-point interactions by taking the interaction energies for the eight different star configurations ϵ_{ijkl} to be different from the sum of pairwise interactions. First, we will consider the case that only those star configurations are affected by relaxation effects, having an occupied central site as well as one or more peripheral
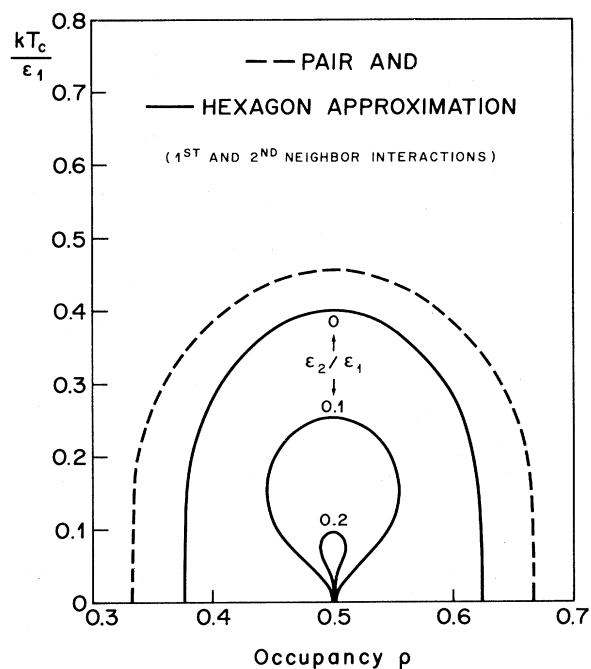
FIG. 9. Phase diagram in the CV approximation with a hexagon as a basic cluster and first- and second-neighbor interactions (ϵ_1, ϵ_2) as compared to the phase diagram in the pair approximation.

sites. This situation is met if the framework ions are rigid and unpolarizable, so that the configurations, having a central empty site, are not affected by relaxation effects. Instead of using the energy parameters relevant to this problem as such, i.e., ϵ_{1111}, ϵ_{1110}, and ϵ_{1100}, it is more convenient for the discussion of the asymmetry of the phase diagram to use the average first-neighbor interaction for a particular configuration,

$$\epsilon_p(3) = \epsilon_{1111}/3, \quad \epsilon_p(2) = \epsilon_{1110}/2, \quad \epsilon_p(1) = \epsilon_{1100} ,$$

(24)

where the variable n in $\epsilon_p(n)$ denotes the number of first-neighbor pairs of particles in the configuration. In addition, we define the asymmetry parameters,

$$\delta_p(i) = \frac{\epsilon_p(i)}{\epsilon_p(1)} - 1 .$$

(25)

The above parameters might be calculated by minimizing the total energy for a particular configuration with respect to the relative positions of the particles, with respect to the minima of their potential wells, if the functional form of the background and interaction potential were known. For instance, for harmonic potential wells and a hard-core interaction there will be an increase in the average pair interaction with the number of pairs. If there are large anharmonic contributions, as is usually the case in solid electrolytes, the increase will be considerably smaller. Because we do not know much about these potential functions, we will assume that the average pair interaction $\epsilon_p(n)$ increases (or decreases) proportionally to the number

of pairs of particles n, so that $\delta_p(3) = 2\delta_p(2) = 2\delta_p$. In Fig. 10 the phase diagram for different values of the asymmetry parameters δ_p are shown. For an increasing average pair interaction with the number of particle pairs or a positive δ_p, the phase diagram becomes narrower, for a negative δ_p it becomes broader. The slope of the phase diagram at $\rho = \frac{1}{2}$ is not very different from zero, except for large and positive δ_p. Another important feature of the phase diagrams of Fig. 10 is that the deviations with respect to the symmetric case are mainly on the high-density side. The reason is that the star configurations responsible for these many-body corrections are high-density configurations. Below the half-filled lattice the probability to find these configurations is small anyhow and their contributions to the free energy are not very significant.

The reverse effect, i.e., a broadening or narrowing of the phase diagram at the low-density side results if the role of the occupied and empty sites is interchanged in the above calculation. In this case the effective interactions for the star configurations with an occupied central site are equal to the sum of the constituent first-neighbor pair interactions, i.e., the parameters $\delta_p(n)$ are zero. Instead different effective average hole-pair interactions $\epsilon_h(n)$ and nonzero asymmetry parameters $\delta_h(n)$ are introduced. This situation can be realized if one allows for relaxations of the framework of nonconducting ions around large clusters of holes. For the same values of the corresponding asymmetry parameters $\delta_h(3) = 2\delta_h(2) = 2\delta_h$ the phase diagrams obtained are just the mirror images of the ones shown in Fig. 10 with respect to the half-filled lattice.

Next we will consider the phenomenon of configuration quenching in solid electrolytes. If the displacement of a
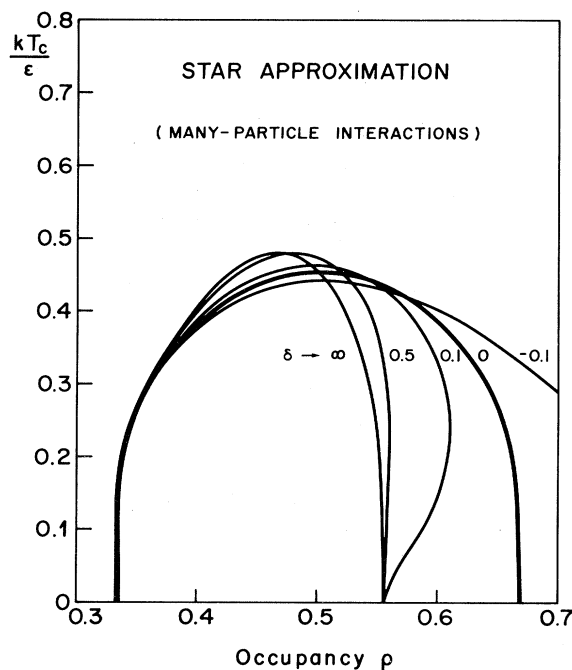

FIG. 10. Phase diagram in the CV approximation with a star as the basic cluster and many-particle interactions. A linear increase (or decrease) of the average pair interaction $\epsilon(n)$ with the number of first-neighbor pairs of particles n is assumed, i.e., $\delta = \epsilon(2)/\epsilon(1) - 1 = \epsilon(3)/\epsilon(2) - 1$.

particle in a particular configuration is equal to or larger than the distance between the lattice site and the position of the potential barrier to a neighboring site, the configuration becomes unstable and has to be discarded from the calculation by setting the corresponding probability to zero.

As a first example we will again assume that the framework of nonconducting ions is rigid and, in addition, that the star configurations with two or three first-neighbor pairs of ions are unstable or

$$s_{1111} = s_{1110} = 0 . \tag{26}$$

All ϵ_{ijkl} can be taken to be zero, except $\epsilon_{1100} = \epsilon_1$. For this case it is possible to derive an analytical expression for the phase diagram. From Eqs. (16) and (26):

$$s^{\alpha}_{1100} = s^{\beta}_{1100} = y_{11} , \tag{27a}$$

$$s^{\alpha}_{1000} = y_{10} - 2y_{11}, \quad s^{\beta}_{1000} = y_{01} - 2y_{11} . \tag{27b}$$

By inserting the above star-configuration probabilities in the superposition equations (17), a set of equations containing only pair probabilities is obtained. From the remaining superposition equations (those for the star configurations with an empty central site), the star-configuration probabilities can be eliminated as well by a factorization similar to the one in Eqs. (20) and (21). The result is Eq. (23) for $i = 0$. Elimination of the a_{ij} and μ from these equations eventually leads to two independent equations for the pair and point probabilities:

$$\frac{y_{01} - 2y_{11}}{y_{10} - 2y_{11}} = \left[\frac{x^{\alpha}_0}{x^{\beta}_0} \right]^2 \tag{28a}$$

and

$$\frac{y_{00}y_{11}}{(y_{10} - 2y_{11})(y_{01} - 2y_{11})} = \exp\left[\frac{-\epsilon_1}{k_B T} \right] . \tag{28b}$$

The two independent parameters may be chosen as x_1 and y_{11}. The remaining parameters can be expressed in the independent ones by using the subsidiary conditions (10) and the condition that the composition is fixed, i.e.,

$$x^{\alpha}_1 + x^{\beta}_1 = 2\rho . \tag{29}$$

From Eqs. (28) the critical temperature can be calculated by requiring that the derivative with respect to the order parameter $\zeta = (x^{\alpha}_1 - x^{\beta}_1)/2$ vanishes, resulting in the condition that

$$y_{11} = \tfrac{1}{2}\rho - \tfrac{1}{6} \tag{30}$$

at the critical temperature. Insertion of this condition in Eq. (28b) yields the following expression for the phase diagram:

$$\frac{\epsilon_1}{k_B T_c} = \ln\frac{9(1-\rho)^2}{(5-9\rho)(3\rho-1)} . \tag{31}$$

This phase diagram is also shown in Fig. 10. Note that the above example of configuration quenching gives results identical to the case of an infinitely large asymmetry parameter δ_p, i.e., for infinitely high interaction energies for star configurations containing two or three first-neighbor pairs of particles, although the underlying phys-

ics is different. The lower phase boundary at 0 K is unchanged with respect to the pair approximation, but the upper phase boundary is shifted to a considerably lower value $(\rho = \tfrac{5}{9})$.

If, on the other hand, large clusters of empty sites are unstable, or if

$$s_{0000} = s_{0001} = 0 , \tag{32}$$

the phase diagram is again the mirror image with respect to the half-filled lattice. Replacing ρ in Eq. (31) by $1-\rho$, we have

$$\frac{\epsilon_1}{k_B T_c} = \ln\frac{9\rho^2}{(9\rho-4)(2-3\rho)} . \tag{33}$$

Finally, we consider the case that both large clusters of particles and large clusters of holes are unstable, i.e., Eqs. (26) and (32) are both satisfied. Then a similar derivation gives

$$\frac{\epsilon_1}{k_B T_c} = \ln\frac{(\rho - 3y_0)^2(5\rho - 3y_0 - 2)^2}{(\rho - y_0)^2 y_0(1 - 2\rho + y_0)} \tag{34a}$$

with

$$y_0 = \frac{21\rho - 8 - [(21\rho - 8)^2 - 21(9\rho^2 - 4\rho)]^{1/2}}{21} . \tag{34b}$$

Obviously, a symmetrical phase diagram is obtained, but much narrower than the one in the pair approximation (see Fig. 11). The phase boundaries are at $\rho = \tfrac{4}{9}$ and $\tfrac{5}{9}$ and $k_B T_c / \epsilon_1 = 0.5098$ at $\rho = \tfrac{1}{2}$.
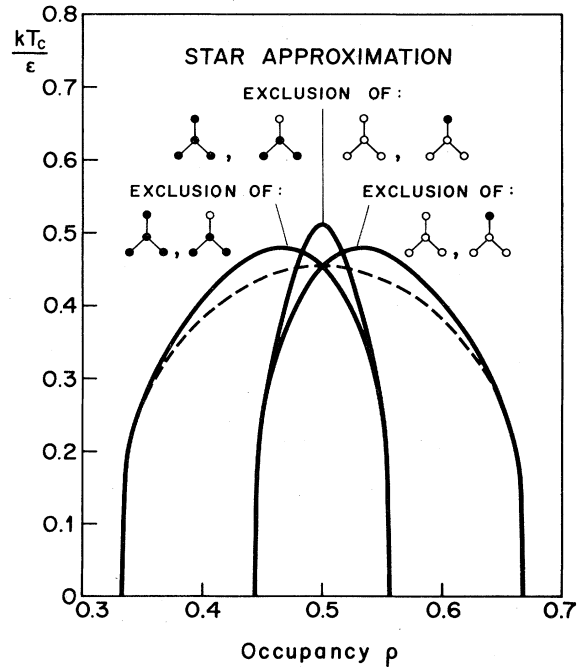

FIG. 11. Phase diagram in the CV approximation with a star as the basic cluster, and exclusion of three- and four-point clusters of particles, vacancies, or both (configuration quenching).

VI. DISCUSSION

A comparison of the calculations of the preceding section with the experimental phase diagram shows that the sign of the slope at the half-filled lattice is correctly reproduced if strong many-body interactions are introduced for three- and four-point clusters of empty sites (Fig. 12). In fact, the steepness of the phase diagram at $\rho = \frac{1}{2}$ suggests that these configurations are unstable.

Strong many-body interactions for the larger clusters of particles, on the other hand, would result in a negative contribution to the slope and therefore cannot be very important. This is a somewhat surprising result at first sight, because, as was pointed out in Sec. IV, it is known that displacement relaxation of the silver ions in AgCrS^2 is very important. One should note, however, that the asymmetry of the phase diagram is not related to the strength of the relaxation effect itself, but rather depends on the relative increase of the average pair interaction with the number of pairs in the relaxed configuration. If there are very strong anharmonic contributions to the background potential, as is the case for AgCrS$_2$, the increase of the average pair interaction with the size of the particle cluster may be rather small, in particular, if the displacements are large. Moreover, it was shown in the preceding section that the relaxation effects in large-particle clusters mainly affect the shape of the phase diagram at the high-density side. Unfortunately, the equilibrium of the AgCrS$_2$-based materials with metallic silver is already reached for silver contents only slightly in excess of 1, and consequently the phase diagram is not known in that region.

The dominating role of the many-body interactions for clusters of empty sites must be related to the relaxation of the framework of nonconducting ions. The sulfur ions next to a local deficiency of conduction ions are expected to be displaced away from the vacant sites, whereas the reverse effect occurs if there is a local excess of conduction ions. These deformations of the framework will modify the background potential for the conduction ions. A local expansion of the lattice most likely will lower the effective potential barriers between a cluster of vacant sites and the neighboring occupied sites, thus destabilizing the low-density clusters. The high-density clusters, on the other hand, will be stabilized by a contraction of the lattice. In agreement with this explanation is the fact that the c parameter becomes shorter at the order-disorder transition temperature.[4] The asymmetry in the distribution of the
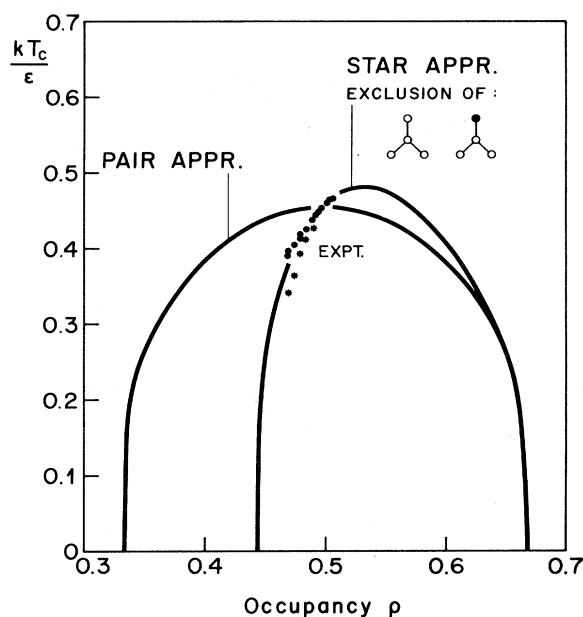

FIG. 12. Qualitative fit of the experimental phase diagram for the silver subsystem in AgCrS$_2$-based materials is obtained if three- and four-point clusters of vacancies are excluded from the CV calculation in the star approximation [Eq. (33)].

holes and particles causes an overall contraction of the lattice in this direction.

In conclusion we have shown that the CV method is a very suitable tool to incorporate relaxation effects in a lattice-gas description of the state of order of a solid electrolyte. Using a relatively simple basic cluster, it has been possible to simulate the strong asymmetric phase diagram of the conduction-ion subsystem of materials with an AgCrS$_2$ type of structure, by including three- and four-body interactions. The sign of the slope of the phase diagram indicates that large hole clusters are suppressed in the disordered state by a destabilizing relaxation of the framework.

[1]H. U. Beyeler et al., in Physics of Superionic Conductors, Vol. 15 of Topics in Current Physics Series, edited by M. B. Salamon (Springer, Heidelberg, 1979), p. 77.

[2]H. U. Beyeler, L. Pietronero, and S. Strässler, Phys. Rev. B 22, 2988 (1980).

[3]R. Kikuchi, Phys. Rev. 81, 988 (1951).

[4]F. M. R. Engelsman, G. A. Wiegers, F. Jellinek, and B. van Laar, J. Solid State Chem. 6, 574 (1973).

[5]T. Hibma, Solid State Commun. 33, 445 (1980).

[6]D. de Fontaine, in Solid State Physics, edited by H. Ehrenreich,

F. Seitz, and D. Turnbull (Academic, New York, 1979), Vol. 34, p. 199.

[7]T. Hibma, Phys. Rev. B 27, 568 (1983).

[8]P. Brüesch, W. Bührer, and T. Hibma, Phys. Rev. B 27, 5052 (1983).

[9]R. Kikuchi, J. Chem. Phys. 60, 1071 (1974).

[10]J. M. Sanchez and D. de Fontaine, Phys. Rev. B 17, 2926 (1978).

[11]C. M. van Baal, Physica (Utrecht) 64, 571 (1973).

[12]R. Kikuchi, J. M. Sanchez, D. de Fontaine, and Hisao Yamau-

chi, Acta Metall. 28, 651 (1980).

[13]J. M. Sanchez and D. de Fontaine, Phys. Rev. B 25, 1759 (1982).

[14]R. M. Fowler and E. A. Guggenheim, *Statistical Mechanics* (Cambridge University, Cambridge, 1960).

[15]J. Hijmans and J. de Boer, Physica (Utrecht) 21 471 (1955); 21,

485 (1955).

[16]R. Kikuchi, J. Chem. Phys. 65, 4545 (1976).

[17]R. M. F. Houtappel, Physica (Utrecht) 16, 425 (1950).

[18]H. Margenau and G. M. Murphy, *The Mathematics of Physics and Chemistry* (Van Nostrand, Princeton, 1956).